

## MATTE-SLAG SEPARATION BEHAVIOR AS A FUNCTION OF IRON PHASE REDUCTION IN COPPER SLAG

Y.-X. Liu <sup>a,b</sup>, Y.-G. Wei <sup>a,b</sup>, S.-W. Zhou <sup>a,b,\*</sup>, B. Li <sup>a,b</sup>, H. Wang <sup>a,b</sup>

<sup>a</sup> Kunming University of Science and Technology, Faculty of Metallurgical and Energy Engineering,  
Kunming, China

<sup>b</sup> Kunming University of Science and Technology, State Key Laboratory of Complex Nonferrous Metal  
Resources Clean Utilization, Kunming, China

(Received 21 April 2022; Accepted 20 December 2022)

### Abstract

The Isa smelting furnace discharges the matte and slag in the same tapping hole. As a result, an electric furnace needs to clean the slag. In the present study, the copper slag cleaning in an electric furnace, particularly the separation of the matte from the slag during the reduction process, was investigated. For  $Fe_3O_4$  to  $FeO$ , the foaming slag in the melt disappeared when the  $Fe_3O_4$  content was less than 10%. With the formation of the metallic iron, the foaming slag formed again, hindering the sedimentation of the matte. When the anthracite dosage increased to 2.61%, the copper content in the slag increased to 9.46%. The microstructure of the slag and the existence of the metallic iron found in the slag were analyzed in detail. The results obtained in this study provide a theoretical basis for the reasonable control of the transformation of  $Fe_3O_4$  during the copper slag cleaning.

**Keywords:** Cleaning; Magnetite; Reduction; Foaming slag

### 1. Introduction

The development of the social economy has brought about a change in the structure of copper consumption. From being used in weapons and tools in prehistoric times, copper is now widely used in telecommunications, electrical and electronic manufacturing, construction, transportation, and other industrial fields, where the consumption of copper is only lower than that of aluminum and iron [1]. The techniques of copper production are divided into hydrometallurgy and pyrometallurgy methods, where its industrial production shows that pyrometallurgical copper smelting technology has the advantages of high efficiency, strong adaptability, and low energy consumption, with 80% of the world's copper produced by pyrometallurgy [2-4]. Meanwhile, the smelting slag produced by pyrometallurgy has stable properties, and the valuable metals in the slag could be recovered [5]. With the development of smelting technology, the oxygen-enriched smelting technologies, with flash smelting and bath smelting have become the mainstream, which alleviated the disadvantages of traditional matte smelting process [6-8].

Oxygen-enriched smelting technology, which

increases the driving force of sulfur-oxygen transfer, allows solid materials to react strongly with both gas/liquid phases and achieves the efficient production of copper matte [9, 10]. The high oxygen potential of the smelting process removes iron from the material to improve the grade of matte, but part of the iron phase over-oxidation would precipitate a high melting point  $Fe_3O_4$  phase, leading to the increased viscosity of the copper slag and deteriorating the slag-matte separation conditions [11-14]. The Isa furnace is a typical representative of oxygen-enriched bath smelting, where the smelting process is a cyclical release of a mixture of copper matte and slag [15, 16]. The slag studied in this paper is an Isa slag. Therefore, the slag cleaning furnace becomes a key supporting process for this melting technology, which aims to reduce  $Fe_3O_4$  in the copper slag and decrease the loss of mechanically entrained copper and chemically dissolved copper in the slag. The reduction is the most direct way to reduce  $Fe_3O_4$  in the slag by adding a reductant. The generated  $FeO$  phase is combined with  $SiO_2$  to form a low melting point fayalite phase, which improves slag fluidity [17-20]. Zhou et al. [21] investigated the metallic copper settling from converter slag during the reduction process, showing that adding the appropriate reductant for the reduction  $Fe_3O_4$  into  $FeO$  was beneficial to copper settling from

\*Corresponding author: swzhou90@126.com



converter slag. Nevertheless, converter slag is usually returned to the smelting furnace for processing. Zheng et al. [22] used rubber seed oil instead of diesel as a reductant for copper slag cleaning. It was demonstrated that the high-temperature cracking products ( $H_2$ , CO, and C) of the rubber seed oil could be used to reduce the magnetite to FeO in the slag.

For current investigations of copper slag cleaning in an electric furnace, some limitations still exist when it comes to explaining the magnetite reduction limit. By recognizing the limitations of the matte settling during reduction, this study aims to clarify the separation of matte particles with the evolution of the iron phase during reduction process. The factors hindering the slag-matte separation were determined, and the deteriorating effect of metallic iron relative to slag properties was also investigated in detail.

## 2. Experimental

### 2.1. Materials

#### 2.1.1. Isa smelting copper slag

The Isa smelting copper slag used in the experiments was obtained from the local copper industry. In the pre-treatment stage, the raw material was ground until it could pass through a 60-mesh sieve. The chemical analysis results of the slag are shown in Table 1. The copper and sulfur contents of the copper slag were 17.82 and 8.07 wt.%, respectively, and the  $Fe_3O_4$  content was 12.9 wt.%. The iron-silicon ratio ( $Fe/SiO_2$ ) was calculated to be 1.73.

Figure 1 shows the X-ray powder diffraction (XRD) pattern of the copper slag. Fayalite, magnetite,

and matte phase could be observed. However, CaO, MgO, and  $Al_2O_3$  were not examined in the plots due to the formation of a glass phase with  $SiO_2$  at high temperatures, which is a non-crystalline substance and cannot be detected by XRD means.

Figure 2 shows the microstructure and energy dispersive X-Ray spectroscopy (EDS) of each phase in the slag sample. It can be observed that the copper slag was mainly present in four phases with different shades of color. Combined with the energy spectrum analysis, fayalite was the matrix of copper slag, which crystallized well during the cooling process and had a bar shape morphology. The brightest-colored substance was mainly composed of a copper-iron-sulfur cluster, i.e., matte, which exhibited a large particle size and quantity. Small matte particles were attached between the magnetite particles. The phase with the darkest color and its shape distribution was

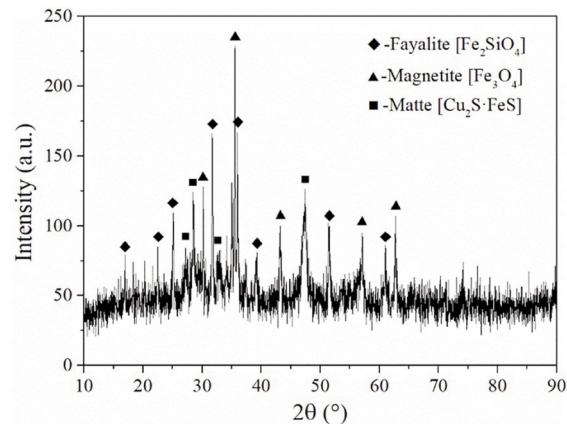


Figure 1. XRD pattern of the copper smelting slag

Table 1. Chemical analysis of the copper smelting slag

| Component      | Cu    | Fe (Total) | $SiO_2$ | S    | $Al_2O_3$ | CaO  | MgO  | Zn   | $Fe_3O_4$ |
|----------------|-------|------------|---------|------|-----------|------|------|------|-----------|
| Content (wt.%) | 17.82 | 33.06      | 19.13   | 8.07 | 2.96      | 2.12 | 1.95 | 1.83 | 12.9      |

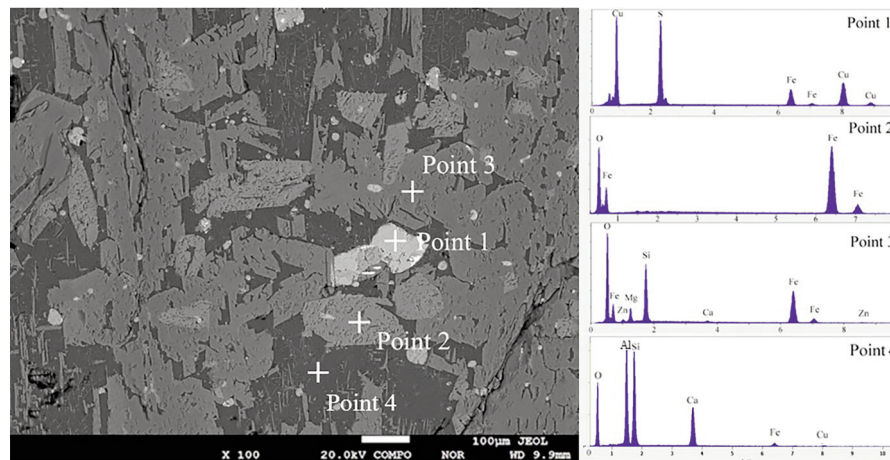


Figure 2. Microstructure and EDS analyses of copper smelting slag



the glass phase. The scanning electron microscope (SEM) analysis results showed that the matte in the slag was mainly interspersed among the phases in the slag.

### 2.1.2. Anthracite

Anthracite was used as a reductant, and its chemical composition is provided in Table 2. The fixed carbon of this anthracite was 76.43 wt.%.

**Table 2.** Proximate analysis of the reductant

| Properties     | Fixed Carbon | Volatile matter | Ash   | Moisture |
|----------------|--------------|-----------------|-------|----------|
| Content (wt.%) | 76.43        | 7.78            | 15.29 | 1.02     |

## 2.2. Experimental method

### 2.2.1. Experimental procedures

The experiments were carried out in a vertical resistance heating furnace using corundum crucibles. The slag samples were homogeneously mixed with different amounts of anthracite and transferred to a corundum crucible. The crucible was placed in the constant temperature zone of the furnace, then the gas in the furnace was emptied, and nitrogen was introduced at a rate of 100 mL/min. Subsequently, the slag samples were heated at a rate of 10 °C/min to 1250 °C, and a constant temperature was maintained for a period of time. After the experiments, the slag sample with crucible were taken out from the furnace at high temperature; then the crucible was put into the water quickly to achieve rapid cooling. Notably, the water level should be well controlled to avoid direct contact between the sample and water. After cooling, the slag was collected for chemical analysis, magnetic analysis, XRD and electro-probe microanalysis (EPMA).

The experimental parameters are listed in Table 3. Test I was an experiment without adding anthracite; Test II was the reduction experiments of copper slag by adding proper anthracite; and Test III was the reduction experiments of copper slag by adding excess anthracite.

**Table 3.** Experimental parameters

|          | Anthracite Addition(g)               | Slag Wt.(g) | Temp. (°C) | Time(min) |
|----------|--------------------------------------|-------------|------------|-----------|
| Test I   | ---                                  | 70          | 1250       | 10        |
| Test II  | 0,0.07,0.13,0.26,0.39,0.46,0.52,0.79 | 70          | 1250       | 10        |
| Test III | 1.05,1.31,1.57,1.83                  | 70          | 1250       | 10        |

### 2.2.2. Experimental devices

The experiments were performed in a vertical resistance heating furnace (Mita Electric Furnace Co., Ltd, Xiangtan, China), and the schematic diagram of experimental device was shown in Figure 3. The samples were ground, and the magnetite content was obtained by measurement on a Satmagan S135 instrument with an accuracy of 0.4 wt.% of the measured value. For mineralogical characterization of the slag samples, the solid phase was confirmed using a Rigaku D/max-R diffractometer (Rigaku MiniFlex 600, Japan). Diffractograms were measured over a 120-min range from 20 to 80 degrees and using steps of 0.01 degrees (operating at 40 kV and 40 mA). To obtain information on the microstructure and composition distribution of the slag samples, the EPMA analysis was performed using a JOEL JXA 8230 equipped with energy-dispersive X-ray spectroscopy. The viscosity of copper slag samples was analyzed by high temperature viscometer (Rheotronic II, Theta), and the temperature measurement range was 1160 °C~1350 °C. Furthermore, the ternary phase diagrams of the FeO-Fe<sub>3</sub>O<sub>4</sub>-SiO<sub>2</sub> and Fe-Cu<sub>2</sub>S-FeS systems at different temperatures were calculated and plotted using the phase diagram module in the FactSage 7.2 thermochemical software.

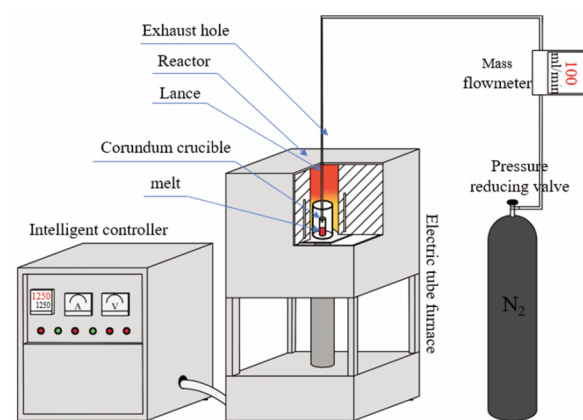


**Figure 3.** The vertical resistance heating furnace

## 3. Results and discussion

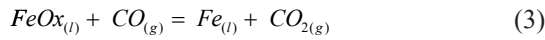
### 3.1. Reduction of Fe phase

The carbon reduction of iron oxides involves direct reduction and indirect reduction. Direct reduction means that carbon is used directly as a reductant to convert high valent iron oxides to low valent iron oxides. Since carbon gasification consumes CO<sub>2</sub>, the direct reduction reaction equation is usually as shown below and it is a strong heat absorption reaction.





When the carbon reduction of iron oxide reaches equilibrium, the other reactions in the system reach equilibrium at the same time, as shown in reactions (2) and (3).



It follows that the CO produced by carbon vaporization would again participate in the oxide reduction, with CO playing a role in transferring the oxygen from the iron oxide to C. While in the presence of carbon, the low concentration of CO<sub>2</sub> in the system enhances the reduction capacity of CO. Therefore, at high temperatures, CO is directly involved in the reaction as the main reducing agent in the carbon reduction process. The thermodynamic equilibrium diagram of the solid carbon reduction of iron oxide can be composed of the thermodynamic equilibrium curves of the carbon gasification reaction together with the indirect reduction reaction of iron oxide, as shown in Figure 4. From the thermodynamic analysis, at temperatures above 702 °C, metallic iron is the stable existing phase of the reaction system (the green region in the figure). The sequence of Fe<sub>2</sub>O<sub>3</sub> reduction transformation is Fe<sub>2</sub>O<sub>3</sub>→Fe<sub>3</sub>O<sub>4</sub>→FeO→Fe, so the amount of reducing agent and kinetic conditions should be controlled to avoid the generation of metallic iron. Furthermore, when the system temperature is below 658 °C, the sequence of Fe<sub>2</sub>O<sub>3</sub> reduction transition is Fe<sub>2</sub>O<sub>3</sub>→Fe<sub>3</sub>O<sub>4</sub> or Fe→FeO→Fe<sub>3</sub>O<sub>4</sub>, and Fe<sub>3</sub>O<sub>4</sub> is the stable region, so Fe<sub>3</sub>O<sub>4</sub> cannot be reduced to FeO.

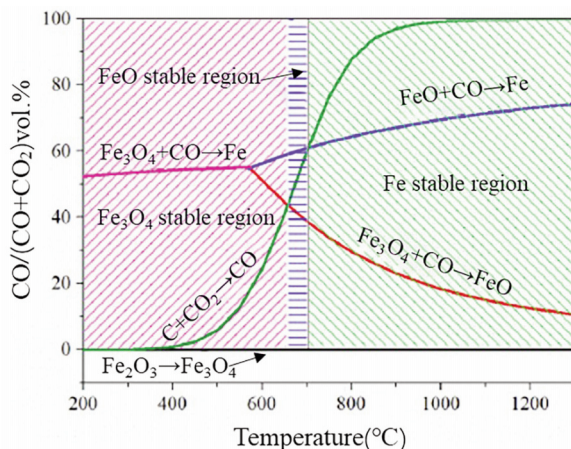


Figure 4. Equilibrium diagram of reduction of iron oxide by C

By adding an appropriate amount of C, the magnetite would be reduced into FeO, so the slag component shifts to the liquid area in the SiO<sub>2</sub>-FeO-

Fe<sub>3</sub>O<sub>4</sub> ternary system as shown in Figure 5, which is conducive to the separation of copper from slag. Without adding a small amount of C, the slag component falls in the *Liq+Spinel+SiO<sub>2(S4)</sub>* phase, indicating poor slag fluidity. By continuing to add the C, the slag component point moves to the *Slag-Liq* phase, avoiding the precipitation of spinel and SiO<sub>2</sub>. When an excessive amount of C is added, the slag forms a metallic Fe phase and the viscosity increases again.

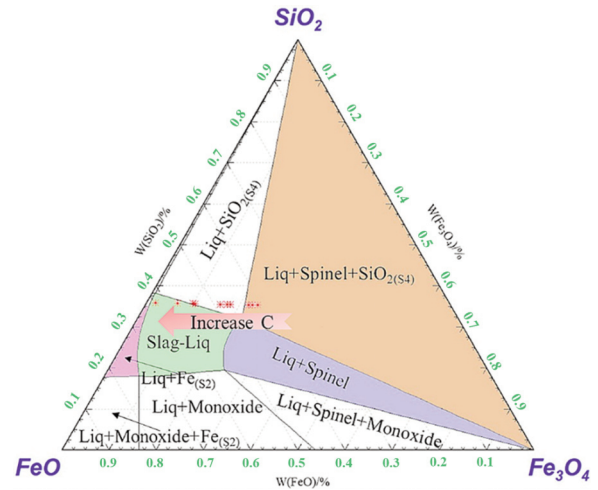


Figure 5. Ternary diagram of SiO<sub>2</sub>-FeO-Fe<sub>3</sub>O<sub>4</sub> at 1250 °C

### 3.2. Separation behavior of copper from slag

The oxygen-enriched smelting technology brings efficient matte production while generating a high melting point Fe<sub>3</sub>O<sub>4</sub> phase. The Isa smelting slag used in this experiment contained 12.9 wt.% of Fe<sub>3</sub>O<sub>4</sub>. Since Fe<sub>3</sub>O<sub>4</sub> was present in solid form at 1250 °C, it led to an increase in slag viscosity. In addition, the increase in slag viscosity enhanced the mechanical entrainment loss of copper. Therefore, to improve the recovery of copper, the reduction of magnetite was inevitable in the process of copper slag cleaning.

#### 3.2.1. Isa slag high-temperature settling experiment

The vertical section of copper slag after high-temperature direct settling separation is shown in Figure 6 (A). It can be observed that the samples had three macroscopic morphologies. The upper structure of the sample was loose with many holes. The lower structure was dense, and two different phases could be observed (regions 1 and 3), as well as yellow-red matter with metal luster (region 2).

Figure 6(B) shows the XRD patterns of each macroscopic morphology. It can be seen from Figure 6 that the substance with a yellow-red and metallic

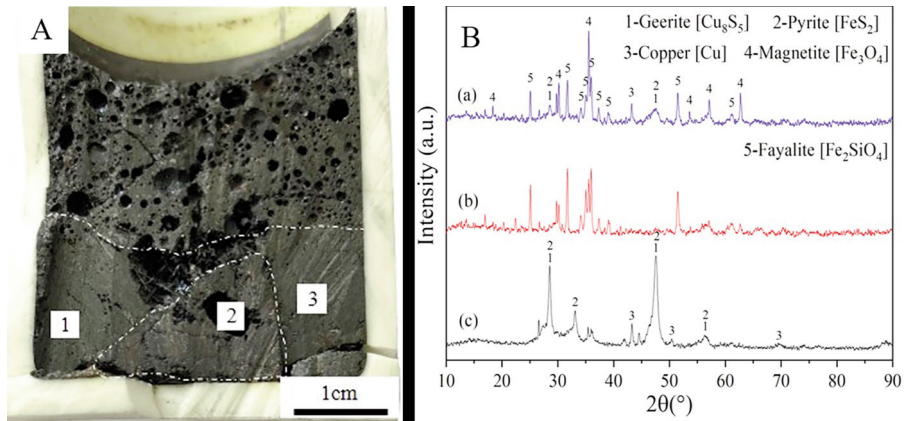


**Figure 6.** (A) Image of the vertical section of the sample after separation at high temperature; (B) XRD patterns of copper smelting slag after separation: (a) foaming slag phase, (b) compact slag phase, and (c) matte phase

luster in the sample (region 2) was the matte phase (Figure 6(Bc)); the upper material with the loose structure and the lower material with the dense structure were both slag phase (Figure 6(Bab)); and the diffraction peaks of the samples with structurally sparse layers were dominated by  $Fe_3O_4$ , followed by fayalite and matte diffraction peaks (Figure 6(Ba)). On the other hand, the diffraction peaks of samples with dense structured slag layers were dominated by fayalite, followed by  $Fe_3O_4$  diffraction peaks. It was difficult to detect matte diffraction peaks. Subsequently, the magnetic analyzer analysis showed that the  $Fe_3O_4$  content in the loose layer slag was 18.1 wt.% and in the dense layer slag it was about 9.3 wt.%, which was completely consistent with the XRD pattern analysis. However,  $Fe_3O_4$  (smelting point 1593 °C) was difficult to melt at current experimental or industrial cleaning temperatures (1200~1300 °C), resulting in the increase of slag viscosity and the change of upper slag structure. Reaction (4) shows that part of  $Fe_3O_4$  in the copper slag would react with

$Cu_2S$  to produce  $SO_2$  gas. In the process of gas escape, it was easy for high viscosity copper slag to form a foaming slag phase. Therefore, high  $Fe_3O_4$  caused the copper slag to produce foaming slag in the process of direct separation at high temperature, which led to the difficulty of slag-matte separation and the increase of the liquid level of molten slag. In actual production, the production of foam slag could even lead to splash accidents.



To further confirm the micromorphology of the microscopical substances in Figure 6(Ba), the SEM and energy dispersive spectrum analyses were carried out for each substance. The results shown in Figure 7(a), (b), and (c) correspond to the upper loose structure slag, lower dense structure slag, and copper matte in Figure 6(Ba). This was confirmed by the energy spectrum that the slag is similar to the original copper slag, and there were four distinct phases in the

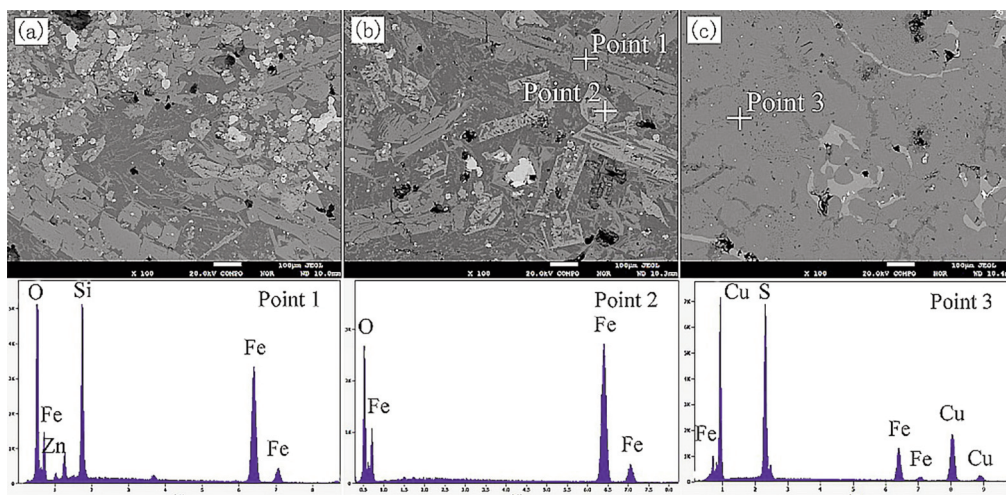


**Figure 7.** Microstructure and EDS analyses of copper smelting slag after separation: (a) the upper loose structure of slag, (b) the lower dense structure of slag, and (c) the copper matte



slag after melting, namely matte, magnetite, fayalite, and glass phase. Compared with Figure 7(b), there was more matte and  $\text{Fe}_3\text{O}_4$  than in Figure 7(a). This also explained how the matte diffraction peak could be observed in Figure 6(Ba), but it was difficult to find in Figure 6(Bb). Part of the reason was due to the interference of the copper target of the detection equipment, but it was mainly due to the small amount of copper matte in the sample. Figure 7(c) shows the matte phase morphology, the Cu-Fe-S was the matrix because the matte had a strong affinity for other metal elements, such as lead and zinc [23]. Therefore, the bright substance in Figure 7(c) was mainly lead.

The effect of  $\text{Fe}_3\text{O}_4$  on smelting can be attributed to the following two aspects: (i) high melting point of  $\text{Fe}_3\text{O}_4$  which existed in the form of a solid phase at smelting temperature. Based on Einstein equation (5), increasing  $\text{Fe}_3\text{O}_4$  caused the viscosity of the copper slag to increase linearly, while the high viscosity copper slag increased the loss of copper entrainment; (ii) The precipitation of  $\text{Fe}_3\text{O}_4$  indicated that the oxygen potential of copper slag was high, which led to the increase of the chemically dissolved copper loss in the copper slag. Therefore, reducing the content of  $\text{Fe}_3\text{O}_4$  in the copper slag by cleaning in an electric furnace was beneficial for improving the copper direct recovery in the smelting process [24].

$$\eta = \eta_s \left(1 + \frac{5}{2}f\right) \quad (5)$$

where  $\eta$  is fluid viscosity containing solid particles,  $\eta_s$  is pure liquid fluid viscosity, and  $f$  is solid volume fraction in the fluid.

### 3.3. Smelting Reduction for $\text{Fe}_3\text{O}_4$

#### 3.3.1. Reducing $\text{Fe}_3\text{O}_4$ to FeO

Figure 8 shows the vertical section of the sample in the crucible after reduction with different amounts of anthracite at 1250 °C for 10 min. With the addition of anthracite, the sample structure changed significantly, the melt was stratified, and the matte settled to the bottom of the melt. Adding 0.1 wt.% of anthracite, the crucible had a thin matte layer at the bottom, as shown in Figure 8(b). Compared with Figure 8(a), the macro morphology of the slag changed after reduction (Fig. 8b). The upper layer of slag was loose, and the pores were larger than those in Figure 8(a). Rapid cooling made the copper slag maintain the molten structure. Fixed carbon in anthracite participated in  $\text{Fe}_3\text{O}_4$  reduction to produce CO and  $\text{CO}_2$  gas. The CO,  $\text{CO}_2$ , and  $\text{SO}_2$  gas that escaped left pores in the copper slag, leading to the copper slag foaming [25]. Similarly, this phenomenon still existed in the experimental samples with anthracite additions of 0.18 and 0.37 wt.%. Based on the theoretical analysis, the reduction reaction in the melt was strengthened with the increase of anthracite content. When the anthracite content increased from 0.1 to 0.37 wt.%, the  $\text{Fe}_3\text{O}_4$  content in the copper slag decreased from 14.27 to 12.56 wt.%, while the corresponding copper content in the slag decreased from 14.03 to 7.61 wt.% (Figure 8). The phenomenon indicated that the foaming slag would be formed when the content of  $\text{Fe}_3\text{O}_4$  in the slag became higher than 12.56%, hindering the separation of the slag-matte. Therefore, the thickness of the matte layer at a lower

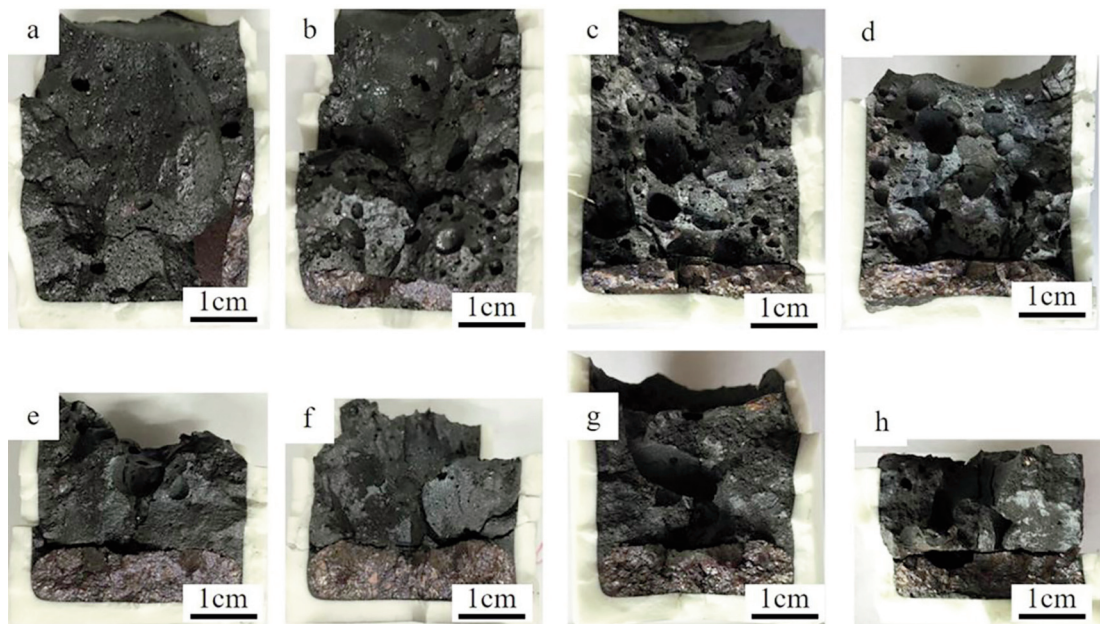


**Figure 8.** Images of the vertical section of the sample in crucible after reduction with various anthracite dosages: (a) 0, (b) 0.1%, (c) 0.18%, (d) 0.37%, (e) 0.56%, (f) 0.66%, (g) 0.74%, and (h) 1.13%

layer of the crucible had a slight change, as shown in Figure 8(b-d).

Further increase of the amount of anthracite caused the foaming slag to disappear, the copper slag structure became dense, and the matte layer was thickened (Figure 8(e-h)). By increasing the anthracite content from 0.56 to 1.13 wt.%, the  $Fe_3O_4$  content in the slag decreased from 8.23 to 1.52 wt.% and copper content decreased from 3.98 to 2.87 wt.% (Figure 9). Therefore, the decrease of  $Fe_3O_4$  in copper slag was conducive to the direct settling and separation of matte particles from slag.

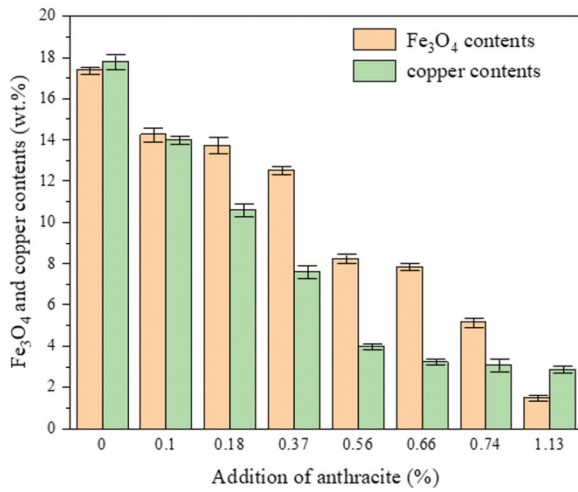


Figure 9. Contents of  $Fe_3O_4$  and copper in slag after reduction with various anthracite dosages

Figure 10 shows the XRD patterns of the samples after reduction with different anthracite contents. The diffraction peak of magnetite gradually decreased with the increase of anthracite content, while the diffraction peak of fayalite increased. The FeO generated from  $Fe_3O_4$  reduction combined with the  $SiO_2$  in the slag to form fayalite, which enhanced the diffraction peak of fayalite (Equations 6 and 7). Therefore, using the saturated  $SiO_2$  slag system in the

smelting could reduce the activity of  $Fe_3O_4$  and reduce its precipitation. The  $Fe_3O_4$  diffraction peak in the copper slag disappeared with the addition of 1.13 wt.% anthracite; the  $Fe_3O_4$  content in the slag was approximately 1.52 wt.%, which made it difficult to be detected by X-ray. Based on the phase diagram of the  $FeO-Fe_3O_4-SiO_2$  ternary system (Figure 5), the slag composition point was located in the slag liquid phase region after reduction, which prevented the foaming slag from forming.

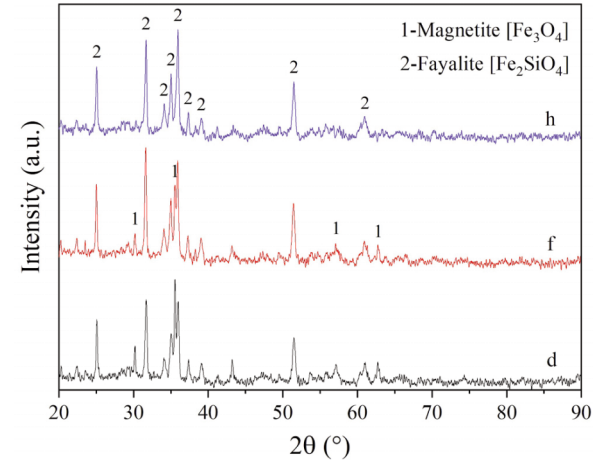


Figure 10. XRD patterns of slag after reduction with various anthracite dosages: (d) 0.37%, (f) 0.66%, and (h) 1.13%

Figure 11 shows the microstructure and energy spectrum analysis of the samples after the reduction of the copper slag with 1.13 wt.% anthracite. The energy spectrum analysis showed that the small white particles were matte particles, while the grey block was the fayalite phase. Because the content of  $Fe_3O_4$  in the sample was only 1.52 wt.%, it was difficult to find it under the condition of low magnification. Without proper settling duration, the fine matte particles were entrained in the slag as a result.

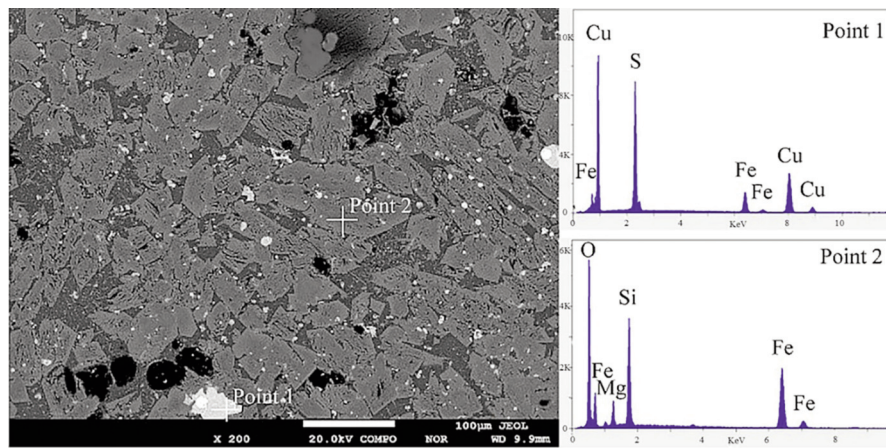
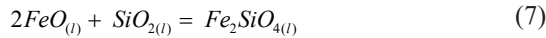
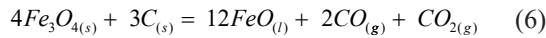


Figure 11. Microstructure and EDS analyses of slag after reduction with 1.13 wt.% anthracite





### 3.3.2. Reducing FeO to Fe

An excessive amount of reductant led to the metallization reduction of  $\text{Fe}_3\text{O}_4$  in the slag. Therefore, part of  $\text{Fe}_3\text{O}_4$  was excessively reduced by adding anthracite to investigate the sedimentation of matte particles in the melt with the metallic iron phase.

Based on the theoretical calculation (Reaction 3), adding 0.66 wt.% anthracite could completely reduce  $\text{Fe}_3\text{O}_4$  to FeO. However, experimental results indicated that the  $\text{Fe}_3\text{O}_4$  content decreased to approximately 7.84 wt.% with the addition of 0.66 wt.% anthracite. Fixed carbon was used as a direct reductant to participate in the reduction reaction, and the solid carbon was converted to CO. Part of CO would exit the reactor along with the tail gas during the reduction process, decreasing the utilization rate of the reductant. In addition, due to the limitation of kinetic conditions, the reaction failed to reach equilibrium in time. When the anthracite content was increased to 1.5 wt.%, the  $\text{Fe}_3\text{O}_4$  content in the slag decreased to 0.78 wt.%. By further increasing the anthracite content, the metallization reduction of  $\text{Fe}_3\text{O}_4$  would occur as a result.

Figure 12 shows the vertical section of the slag sample after reduction with various amounts of anthracite at 1250 °C for 10 min. The  $\text{Fe}_3\text{O}_4$  content in the slag decreased to 0.78 wt.% after reduction with 1.5 wt.% anthracite, and the matte particles settled well, as presented in Figure 12(a). The copper content in the slag after reduction with various anthracite dosages is shown in Figure 13. When the anthracite dosage increased to 1.87 wt.%, the melt still presented good stratification. From a macroscopic observation, the structure of the copper slag exhibited no obvious change, though the copper content of slag increased to 5.04 wt.%. Further increasing the anthracite dosage caused the slag level to rise, whereas the thickness of the matte layer at the bottom of the crucible decreased (Figure 12(c-d)). This phenomenon was more obvious under the addition of

2.61 wt.% anthracite (Figure 12(d)), at which the copper content in the slag continued to increase to 9.46 wt.%.

Through the viscosity measurement of the original slag and the over-reduced copper slag, it was found that when the copper slag was over-reduced to form metal iron, the viscosity of the slag increased again, which was even higher than that of the original copper slag, as shown in Figure 14. This indicated that the increase in iron content in the slag once again led to the formation of foaming slag, which was not conducive to slag-matte separation.

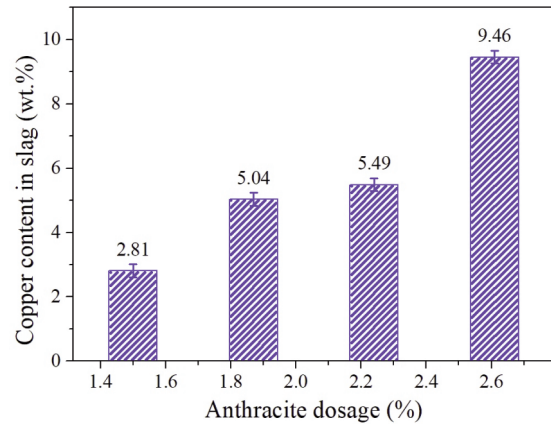


Figure 13. Copper content in slag after reduction with various anthracite dosages

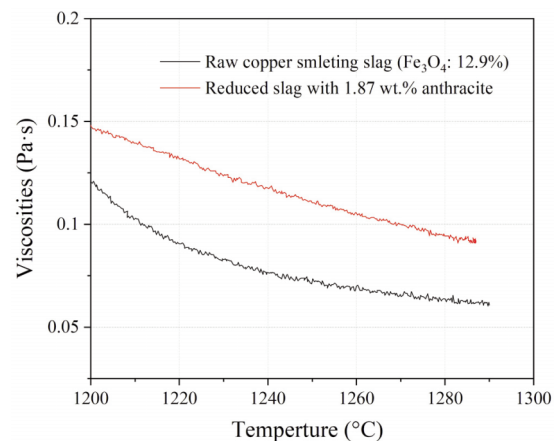


Figure 14. Viscosities of the raw copper smelting slag and reduced slag with 1.87 wt.% anthracites

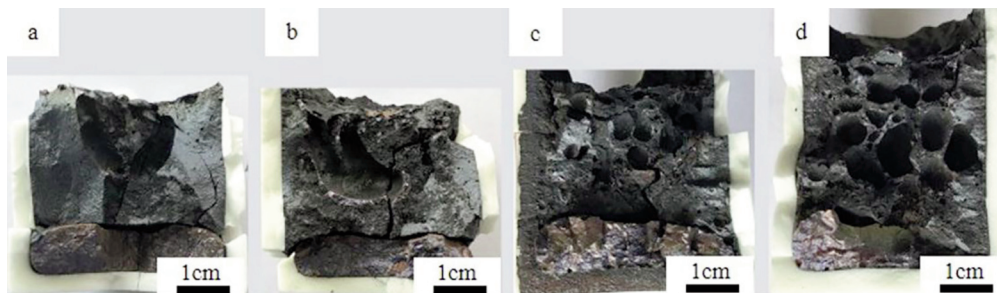


Figure 12. Images of the vertical section of the sample in the crucible after reduction with various anthracite dosages: (a) 1.5 wt.%, (b) 1.87 wt.%, (c) 2.24 wt.%, and (d) 2.61 wt.%

Figure 15 shows the overall microstructure of the upper foaming slag after over reduction (anthracite dosage of 2.61 wt.%). Many matte particles in the slag were distributed in the phase boundary, namely, the copper slag pore boundary. No  $Fe_3O_4$  particles were found. Then, the interface area of the copper matte slag was analyzed by EPMA, and the results are shown in Figure 16. In the matte phase, the metallic iron phase could be observed with a rounded granular morphology. From the energy spectrum analysis, the metallic iron contained copper with a content of 6.2 wt.%, indicating that it belonged to a copper-iron alloy phase with a  $\gamma$ -Fe phase as the matrix.

Based on the Fe-Cu<sub>2</sub>S-FeS ternary phase diagram at 1250 °C (Figure 17), the Fe content in the ternary phase above 10 wt.% would cause the precipitation of the Cu-Fe alloy phase in the system. A copper-iron alloy in the matte phase led to an increase of particle density, from this point of view alone, it was conducive to the precipitation and separation of matte particles. However, the copper-iron alloy based on the metallic iron was a high melting point phase, which could not be completely melted at the current experimental temperature (1250 °C). Accordingly, the copper-iron alloys were mainly round particles instead of their shape, indicating their non-melting state. This finding indicated that copper-iron alloys

were similar to  $Fe_3O_4$ , and the alloys existed in the solid form in the slag, while the high melting point phase increased the apparent viscosity of the melt. High-viscosity slag was prone to transforming into foaming slag when bubbles were generated, which simultaneously prevented the sedimentation of copper matte particles [26].

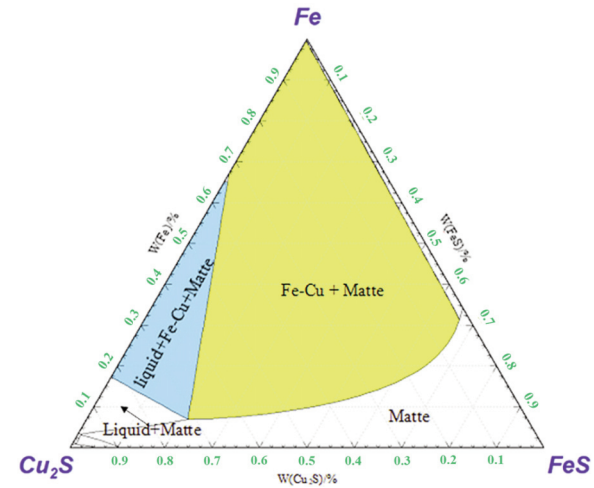


Figure 17. Ternary phase diagram of Fe-Cu<sub>2</sub>S-FeS at 1250 °C

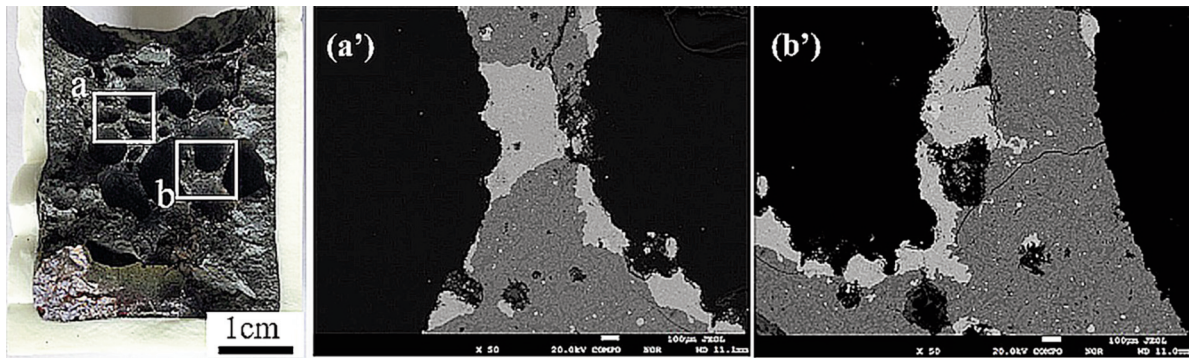


Figure 15. Microstructure of the foaming slag in the upper part of slag after reduction with 2.61 wt.% anthracite, where (a') and (b') are the microstructures of (a) and (b), respectively

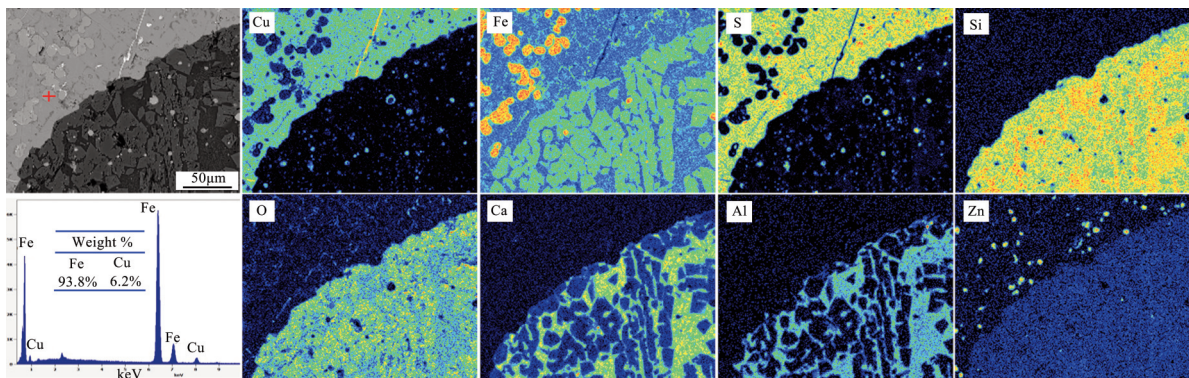


Figure 16. EPMA analysis of the interface area of the matte and slag



#### 4. Conclusions

The copper slag contained approximately 17.82 wt.% copper and 12.9 wt.%  $\text{Fe}_3\text{O}_4$ . At 1250 °C, the slag formed a foaming slag due to the high  $\text{Fe}_3\text{O}_4$  content, which prevented the separation of matte particles from the slag. By adding 1.13 wt.% anthracite, the  $\text{Fe}_3\text{O}_4$  in the slag decreased to 1.52 wt.%, which allowed it to prevent the formation of foaming slag. The iron phase in the slag transformed into metallic iron with an excessive amount of reductant, and the copper-iron alloy was precipitated, which had a high melting point. A large amount of the  $\gamma$ -Fe phase in the slag increased its viscosity, resulting in the formation of foaming slag and hindering the slag-matte separation. During the copper slag cleaning in an electric furnace, a decrease in the content of  $\text{Fe}_3\text{O}_4$  in the slag was beneficial to the separation of slag-matte. Controlling the  $\text{Fe}_3\text{O}_4$  content in the slag at approximately 6% was more conducive to the separation of matte from the slag and the protection of the furnace lining.

#### Acknowledgments

*This work was supported by the National Natural Science Foundation of China (51974142); Autonomous project of State Key Laboratory of Complex Nonferrous Metal Resources Clean Utilization (CNMRCUTS2104).*

#### Author contributions

*Writing-original draft, Investigation, Data curation: Yuxuan Liu. Conceptualization, Writing-review & editing: Shiwei Zhou. Validation: Bo Li. Investigation: Yonggang Wei. Funding acquisition, Supervision: Hua Wang.*

#### Data availability

*The data used to support the findings of this study are available from the corresponding author upon request.*

#### Conflict of interest

*The authors declare that they have no known competing financial interests or personal relationships that could have appeared to influence the work reported in this paper.*

#### References

- [1] K. Nakajima, I. Daigo, K. Nansai, K. Matsubae, W. Takayanagi, M. Tomita, Y. Matsuno, Global distribution of material consumption: Nickel, copper, and iron, *Resources, Conservation and Recycling*, 133 (2018) 369-374. <https://doi.org/10.1016/j.resconrec.2017.08.029>
- [2] H. Tian, Z. Guo, J. Pan, D. Zhu, D. Wang, Comprehensive review on metallurgical recycling and cleaning of copper slag, *Resources, Conservation and Recycling*, 168 (2021) 105366. <https://doi.org/10.1016/j.resconrec.2020.105366>
- [3] X. Guo, M. Tian, S. Wang, S. Yan, Z. Li, Element distribution in oxygen-enriched bottom-blown smelting of high-arsenic copper dross, *The Journal of the Minerals, Metals Materials Society*, 71 (6) (2019) 3941-3948. <https://doi.org/10.1007/s11837-019-03767-3>
- [4] Y. Hongxia, S. Pengfei, Oxygen enriched bottom blowing bath smelting temperature control method based on variable universe fuzzy-PID, *The 6th International Conference on Intelligent Networks and Intelligent Systems*, Jul.24, Shenyang, China, 2014, 127-130. <https://doi.org/10.1109/ICINIS.2013.39>
- [5] A. Habib, H. N. Bhatti, M. Iqbal, Metallurgical processing strategies for metals recovery from industrial slags, *Zeitschrift für Physikalische Chemie*, 234 (2) (2020) 201-231. <https://doi.org/10.1515/zpch-2019-0001>
- [6] J. Wang, M.-Y. Gu, G. Liu, H. Chu, F.-L. Wu, Y. Fang, Y.-W. Tu, W.-K. Li, S. Lan, A thermodynamic regression analysis of oxygen bottom-blown copper smelting furnace based on uniform design method, *Chemical Industry Engineering Progress*, 35 (05) (2016) 1303-1308. <https://doi.org/10.16085/j.issn.1000-6613.2016.05.006>
- [7] S. Degterov, A. Pelton, A thermodynamic database for copper smelting and converting, *Metallurgical and Materials Transactions B*, 30 (4) (1999) 661-669. <http://doi.org/10.1007/s11663-999-0027-4>
- [8] H.-L. Zhao, P. Yin, L.-F. Zhang, S. Wang, Water model experiments of multiphase mixing in the top-blown smelting process of copper concentrate, *International Journal of Minerals, Metallurgy Materials*, 23 (12) (2016) 1369-1376. <https://doi.org/10.1007/s12613-016-1360-7>
- [9] R. Sridhar, J. M. Toguri, S. Simeonov, Copper losses and thermodynamic considerations in copper smelting, *Metallurgical and Materials Transactions B*, 28 (2) (1997) 191-200. <http://doi.org/10.1007/s11663-997-0084-5>
- [10] X. Gao, Z. Chen, J. Shi, P. Taskinen, A. Jokilaakso, Effect of cooling rate and slag modification on the copper matte in smelting slag, *Mining Metallurgy Exploration*, 37 (2) (2020) 1593-1601. <http://doi.org/10.1007/s42461-020-00274-x>
- [11] X. Wan, L. Shen, A. Jokilaakso, H. Eri, P. Taskinen, Experimental approach to matte-slag reactions in the flash smelting process, *Mineral Processing Extractive Metallurgy Review*, 42 (4) (2020) 231-241. <http://doi.org/10.1080/08827508.2020.1737801>
- [12] J.P. Jylh, N.A. Khan, A. Jokilaakso, Computational approaches for studying slag-matte interactions in the flash smelting furnace (FSF) settler, *Processes*, 8 (4) (2020) 485. <http://doi.org/10.3390/pr8040485>
- [13] Q.M. Wang, X.Y. Guo, Q.H. Tian, Copper smelting mechanism in oxygen bottom-blown furnace, *Transactions of Nonferrous Metals Society of China*, 27 (4) (2017) 946-953. [http://doi.org/10.1016/S1003-6326\(17\)60110-9](http://doi.org/10.1016/S1003-6326(17)60110-9)
- [14] D. R. Swinbourne, R. C. West, M. E. Reed,



- Computational thermodynamic modelling of direct to blister copper smelting, *Mineral Processing and Extractive Metallurgy*, 120 (1) (2011) 1-9.  
<https://doi.org/10.1179/1743285510Y.0000000003>
- [15] Y. Chen, Z. Zhao, P. Taskinen, Y. Liang, H. Liu, Characterization of copper smelting flue dusts from a bottom-blowing bath smelting furnace and a flash smelting furnace, *Metallurgical and Materials Transactions B*, 51 (6) (2020) 2596-2608.  
<http://doi.org/10.1007/s11663-020-01907-8>
- [16] X. Li, Y. Liu, D. Wang, T. Zhang, Emulsification and flow characteristics in copper oxygen-rich side-blown bath smelting process, *Metals*, 10 (11) (2020) 1520.  
<http://doi.org/10.3390/met10111520>
- [17] B. Wang, Z. Wang, Y. Jia, H. Yu, Dynamic model of bottom blown oxygen copper smelting process, *International Journal of Modelling Identification and Control*, 30 (2) (2018) 118-131.  
<http://doi.org/10.1504/IJMIC.2018.10014981>
- [18] Q. Zhang, J. Chen, Y. Wu, H. Liu, H. Yang, Suppressing SO<sub>3</sub> formation in copper smelting flue gas by ejecting pyrite into flue, *Environmental Science and Pollution Research*, 28 (2) (2020) 4307-4316.  
<https://doi.org/10.1007/s11356-020-10796-y>
- [19] A. Yazawa, Y. Takeda, Y. Waseda, Thermodynamic properties and structure of ferrite slags and their process implications, *Canadian Metallurgical Quarterly*, 20 (2) (2013) 129-134.  
<http://doi.org/10.1179/000844381795270354>
- [20] P. Chen, H. Xiao, J. Chen, L. Chen, D. Zhang, W. Liu, T. Yang, Oxygen-rich side-blown bath smelting of copper dross: A process study, *Journal of Sustainable Metallurgy*, 6 (2) (2020) 344-354.  
<http://doi.org/10.1007/s40831-020-00278-3>
- [21] S. Zhou, Y. Wei, B. Li, H. Wang, Effect of iron phase evolution on copper separation from slag via coal-based reduction, *Metallurgical and Materials Transactions B*, 49 (6) (2018) 3086-3096.  
<http://doi.org/10.1007/s11663-018-1379-4>
- [22] H. Zheng, B. Li, H. Zhou, Y. Wei, H. Wang, Dilution of copper slag under reduction of rubber seed oil, *The Chinese Journal of Process Engineering*, 19 (3) (2019) 589-596.  
<https://doi.org/10.12034/j.issn.1009-606X.218284>
- [23] S. Sineva, M. Shevchenko, D. Shishin, Phase equilibria and minor element distributions in complex copper/slag/matte systems, *The Journal of the Minerals, Metals Materials Society*, 72 (10) (2020) 3401-3409.  
<http://doi.org/10.1007/s11837-020-04326-x>
- [24] J. Happel, H. Brenner, *Low Reynolds number hydrodynamics*, Kluwer Boston, United States, 1983, 431-474.
- [25] Y. Wei, T. Zhang, B. Li, S. Zhou, Copper smelting slag cleaning in an electric furnace by using waste cooking oil, *Metallurgical and Materials Transactions B*, 51 (B) (2020) 2756-2768.  
<https://doi.org/10.1007/s11663-020-01986-7>
- [26] S. Sineva, P. C. Hayes, E. Jak, Experimental study of the slag/matte/metal (Fe or Cu)/tridymite equilibria in the Cu-Fe-O-S-Si-(Ca) system at 1473 K (1200 °C): Effect of Ca, *Metallurgical and Materials Transactions B*, 52 (2) (2021) 2163-2170.  
<http://doi.org/10.1007/s11663-021-02188-5>

## PONAŠANJE BAKRENCA I ŠLJAKE PRILIKOM ODVAJANJA U BAKARNOJ ŠLJACI TOKOM REDUKCIJE FAZE GVOŽĐA

Y.-X. Liu <sup>a,b</sup>, Y.-G. Wei <sup>a,b</sup>, S.-W. Zhou <sup>a,b,\*</sup>, B. Li <sup>a,b</sup>, H. Wang <sup>a,b</sup>

<sup>a</sup> Univerzitet za nauku i tehnologiju u Kunmingu, Fakultet za metalurško i energetska inženjerstvo, Kunming, Kina

<sup>b</sup> Univerzitet za nauku i tehnologiju u Kunmingu, Glavna državna laboratorija za čisto korišćenje kompleksnih resursa obojenih metala, Kunming, Kina

### Apstrakt

Isasmelt peč ispušta bakrenac i šljaku u isti otvor i zbog toga je potrebno prečistiti šljaku u električnoj peći. U ovom radu je istraživano prečišćavanje bakarne šljake u električnoj peći, gde je posebna pažnja posvećena odvajanju bakrenca od šljake tokom redukcionog procesa. Tokom redukcije Fe<sub>3</sub>O<sub>4</sub> do FeO, penasta šljaka u rastopu se izgubila kada je sadržaj Fe<sub>3</sub>O<sub>4</sub> bio manji od 10%. Sa formiranjem metalne komponente gvožđa, penasta šljaka se ponovo formirala, što je otežalo taloženje bakrenca. Kada je količina antracita povećana na 2,61%, sadržaj bakra u šljaci se povećao na 9,46%. Mikrostruktura šljake, kao i postojanje metalne komponente gvožđa, detaljno je analizirano. Dobijeni rezultati pružaju teorijsku osnovu za određenu kontrolu transformacije Fe<sub>3</sub>O<sub>4</sub> tokom prečišćavanja šljake.

**Ključne reči:** Prečišćavanje; Magnetit; Redukcija; Penasta šljaka

